Next Materials 12 (2026) 102511

Contents lists available at ScienceDirect

Next Materials

journal homepage: www.sciencedirect.com/journal/next-materials

Research article

Dielectric relaxation in polyethylene glycol 400: A scale effect

A.O. Sobchuk [a], V.B. Shevchenko [a], S.A. Alekseev [a], K.S. Yablochkova [a], E.A. Lysenkov [b], R.V. Dinzhos [b,c], Filip Ublekov [c], Neli Koseva [c], P.S. Yaremov [d], O.V. Shvets [d], O.M. Alekseev [a], M.M. Lazarenko [a,*]

[a] Taras Shevchenko National University of Kyiv, Kyiv, Ukraine
[b] Petro Mohyla Black Sea National University, Mykolayiv, Ukraine
[c] Institute of Polymers Bulgarian Academy of Sciences, Sofia, Bulgaria
[d] L. V. Pisarzhevskii Institute of Physical Chemistry of the National Academy of Sciences of Ukraine, Kyiv, Ukraine

ARTICLE INFO

Keywords:
Nanoinclusion
Silica gel
Relaxation Processes
PEG-400
Conformational motion
Scale effect

ABSTRACT

This work reports the dielectric properties of the porous matrix – inclusions system. The porous matrices used were silica gels with different pore sizes. The pores were filled with PEG-400. The synergy of gravimetric method, structural analysis, and the dielectric spectroscopy reveal how the size of the matrix pores affects the parameters of the low-temperature dielectric relaxation of PEG-400. We demonstrate that as the pore size decreases, the influence of the silica gel pore walls on the structure and thermal mobility of PEG 400 inclusions increases. This interaction causes a shift in the dielectric relaxation peak towards higher temperatures for smaller nano-inclusions, along with changes in dielectric relaxation parameters. Notably, the difference in energies between the equilibrium states of the relaxator increases with decreasing pore sizes. This observation can be explained by the fact that one of the relaxator's equilibrium positions is modified by interaction with the pore wall, which behaves differently from typical intermolecular interactions. Moreover, the interaction with the wall reduces the number of relaxators that can be simultaneously activated in a smaller pore, since the energy required for a relaxator to transition to the excited state increases. These characteristics could be beneficial for developing materials with programmable dielectric properties and for designing nanostructured composites with specific temperature- and frequency-dependent dielectric responses.

1. Introduction

When the characteristic size of a material is of nano-scale (less than about 100 nm), new physical and chemical properties become prominent [1–6]. This is due to the increased impact of surface and kinetic effects, which are usually negligibly small at the macroscopic level. When molecules are spatially confined, several changes take place. They include changes in the way molecules are packed, the conformational distribution in the system, and the types of intermolecular interactions (especially hydrogen bonding). These factors alter the relaxation dynamics and the dielectric behavior of the porous matrix–inclusion system [7]. The study of molecular dynamics in nanopores is important for fundamental research and has many practical applications. These nanopores have potential uses in heat-accumulating materials, electrolytes, and membranes, where the properties within confined spaces determine the system's functionality [8,9].

The geometric characteristics of porous matrices (pore size, shape and size distribution, surface fractality) affect dielectric relaxation of the inclusions. The spectral features of $\varepsilon'(\omega, T)$ and $\varepsilon''(\omega, T)$ reflect not only the properties of the substance itself but also its interaction with the surface or the changes in the molecular mobility inside pores [10–12].

Molecules confined in porous glass and silicon matrices are known to exhibit slowed or modified relaxation dynamics. The examples of such changes are the appearance of additional relaxation components or changes in the temperature dependence of characteristic relaxation times. Both are determined by the micro- and mesostructures of the pores and the properties of their surface groups [13].

Molecular dynamics simulations demonstrate that the density of the polymer layer increases near the surface, while an interfacial 1–3 nm layer with slower dynamics appears, and the activation behavior of relaxation processes changes. The authors of [14,15] also report these effects to be temperature-, surface chemistry, and pore geometry

* Corresponding author.
E-mail address: lazmaxs@knu.ua (M.M. Lazarenko).

https://doi.org/10.1016/j.nxmate.2026.102511
Received 16 April 2026; Received in revised form 24 May 2026; Accepted 10 June 2026
Available online 12 June 2026

dependent.

Both current approaches to modelling and recent experimental data on porous systems suggest that interphase behavior can be interpreted as a collection of regions with different characteristic relaxation times: rapid relaxation in the inner bulk parts of the system and slower relaxation in the surface layers. This interpretation can also account for the interphase (Maxwell-Wagner) polarization at non-uniform pore filling [16,17].

Usually, a decrease in pore size leads to an increase in the relative interaction surface area. This, in turn, increases the impact of the slower surface fraction on the overall relaxation signal. At the same time, very thin pores may alter the nature of the principle (α-) relaxation process, as the bulk dynamic is replaced by localized dynamics [18]. Still, relaxation processes are mostly determined by adsorption energy, the hydrophilic or hydrophobic properties of the pore surfaces, pore sizes, and the molecular weight of the polymer inclusions.

Oligoether diols, such as polyethylene glycol (PEG) and polypropylene glycol (PPG), are useful model systems for studying the effects of confined space. This is due to their polar hydroxyl groups, relative chemical inertness, and well-known behavior in bulk phase [19]. The end hydroxyl groups of PEGs give the molecule a non-zero dipole moment (Fig. 1). By studying the temperature and external frequency variation of the real ε' and imaginary ε'' components of the complex dielectric permittivity, researchers can directly evaluate a number of properties of the polymer. These properties include the molecular thermal mobility of the polymer, its degree of its binding to the surface, and the presence/absence of certain relaxation processes.

For instance, in PEG-silica systems, the surface interaction can significantly affect the process of crystallization, the values of the characteristic relaxation times, and the amplitudes of relaxation processes [20]. Furthermore, recent investigations demonstrated that intermolecular interactions between PEG/PPG chains and silica surfaces can alter the hydrogen-bond structure and aggregation processes in silica-containing systems, emphasizing the critical role of polymer–surface interactions in confined environments [21]. Kim et al. report that PEG molecules near inert silica particles form a heterogeneous layer with modified dynamics (the interphase layer being 1–2 nm thick), very different from the molecular dynamics in the bulk. Oligomeric PPG in nanopores exhibits anomalous diffusion and changes in the spectral forms of relaxation; these anomalies depend on pore size (2.5–7.5 nm), indicating a substantial change in segmental dynamics in confined spaces [22].

Despite the presence of numerous studies focusing on phase transition and general thermal dynamic effects in confined spaces, a number of questions remain unanswered. They include, for instance, the relationship between the spectral-temporal characteristics of the dielectric relaxation of the organic inclusions and the size of pores in meso- and micro-porous environments. Another example is the relationship between the above-mentioned characteristics and the nature of the matrix's surface groups.

Although many researchers report that the size of pores affects the relaxation processes, influence of their sizes on the parameters of the relaxation process is underreported. In addition to that, no studies offer the mechanism of how pore size influences the relaxation parameters. In the present work, we want to elucidate the relationship between the size of pores and the dielectric relaxation properties in oligoether diols. In particular, we aim to discuss how the size of the pores of the silica gel matrices affect the parameters of the low-temperature relaxation in PEG−400 – silica gel nanocomposites. All matrices in the present research have the identical chemical composition of the pore surface, but a different mean size of pores.

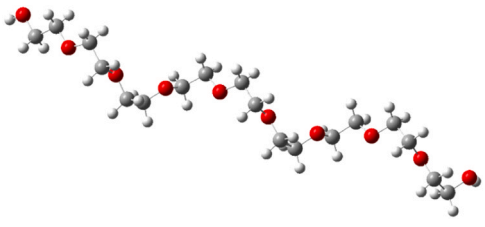

Fig. 1. PEG−400 molecule.

2. Materials and methods

2.1. Materials

The polyethylene glycol PEG−400 with molecular weight Mw ≈ 400 and formula HO[–CH_2–CH_2–O–]$_n$H (where n ≈ 11) was purchased from Fluka. It is an oily, viscous liquid with the density $r_n = 1013\ kg{\cdot}m^{-3}$ at T = 293 K. Before the preparation of other samples and measurements, the PEG sample was heated to T = 373 K for 5 h measurements under stirring, under vacuum, to remove water and other possible volatile impurities.

The choice of PEG−400 was motivated by our previous characterization of its relevant physical properties in [23]. At lower temperatures, PEG−400 is known to form an amorphous-crystalline structure. When heated, it undergoes first a low-temperature and then a higher-temperature relaxation. The lower-temperature dielectric relaxation can be attributed to conformational motion of PEG's *HO-CH_2-CH_2* end groups. In contrast, the higher-temperature dielectric relaxation is caused by the conformational motion in the chain of the PEG molecule, which can arise due to the motion of local topological defects along the chain.

The following silica gels having different pore size were chosen to serve as nanoporous matrices: KCC−4, Silica gel 60 UCT (Sil 60), KCK−2.5, Kieselgel 100 (Sil 100), Silochrome C−120 (CX−120).

Silica gels KCK−2.5 and KCC−4 were ground in a mortar, and a 0.1 mm to 0.315 mm fraction was sieved. To remove impurities and to ensure complete hydroxylation of SiO_2 surface, all silica gels were refluxed in 67% nitric acid for 5–6 h under mechanical stirring. Afterwards the silica gels were thoroughly washed with DI water by decantation to remove dust, followed by washing on a glass filter until neutral pH of the rinse liquid. Finally, the silica gels were dried in air at 200 °C for 4 h in air and stored in tightly closed containers.

To prepare nanocomposites, PEG−400 was first mixed with anhydrous ethanol: 8.33 g of PEG per 25 ml of ethanol to obtain a solution of $1/3\ g{\cdot}ml^{-1}$ concentration. Then, 1 g silica gel samples were placed in small glass vials and 1.5 ml portions of PEG ethanolic solution were added to each. In cases of incomplete wetting of silica gels (KCK−2.5 and CX−120), small amounts of ethanol were added gradually to the samples until full wetting was achieved. Following this, the samples were treated for 15 min in an ultrasound bath, dried at 75 °C and then at 110 °C with intermittent mixing. The final samples were white loose powders.

2.2. Methods

The pore size and surface areas of silica gels were measured by N_2 adsorption at 77 K, using AMI-Micro−300 Series (Altamira instrument Micro300C−02-Analysis Station3) after outgassing the samples under vacuum at 150 °C for 4 h. Textural characteristics were calculated using the standard BET, BJH and t-plot methods, with Altamira 1042 software supplied.

The moisture content was determined by thermogravimetry using a PerkinElmer TGA 4000 Thermogravimetric Analyzer under argon atmosphere. The samples were heated from 20 to 800 °C at the rate of $10\ °C{\cdot}min^{-1}$.

Wide Angle X-ray Diffraction (WAXD) scans were obtained on Bruker D8 Advance ECO diffractometer, operating at 40 kV and 25 mA in Bragg–Brentano geometry with Ni-filtered CuKα radiation and a LynxEye-XE detector over the 2θ range of 10–40° with a scanning rate of

$0.02^{\circ}\cdot s^{-1}$.

The dielectric properties were studied in a 1–50 kHz frequency range and a −196–100 °C temperature range using an automated installation based on a P5083 AC bridge and a four-electrode thermostated cell, with an option for sample thickness control. The samples were placed in enclosed polyethylene capsules, which allowed us to measure them in different states and at a constant water content [24,25].

The bridge method utilized in the study to measure ε*(ω,T) ensures a high resolution of ΔC= 10^{-3} pF, Δtg δ = 10^{-5} and precision of ΔC/C= 0.1%. The frequency range (1–50 kHz) and the simultaneous temperature scanning at 2 K.min^{-1} allowed for the measurements of capacitance and tangent of loss with the step of 1 °C from −190–100 °C while taking into account the changes in the sample thickness due to thermal expansion and deformation.

3. Experimental

3.1. Pore size analysis

To determine the textural characteristics of porous matrices, we applied the N_2 adsorption method. Fig. 2a shows the adsorption/desorption isotherms obtained for the KCC−4, KCK−2.5, and CX−120 silica gels. The behavior of the isotherms for the remaining matrices (Sil−60, Sil−100) is qualitatively similar and is shown in Fig. S1 of the Supplementary Materials. According to the IUPAC classification [26], the nitrogen adsorption/desorption data obtained are IVa isotherms with H1 and H2-type hysteresis loops [27]. The isotherms of this class are typical for silica gels of irregular morphology. The Type H1 (Sil−100, CX−120) loop is found in materials which exhibit a narrow range of uniform mesopores. Hysteresis loops of Type H2 (KCC−4, KCK−2.5, Sil−60) are given by more complex pore structures in which network effects are important.

The pore size distributions (Fig. 2b) for KCC−4 and KCK−2.5 are typical for mesoporous silica gels, while for CX−120 silica the pores are much wider. The pore size distributions of the remaining samples (Sil−60, and Sil−100) shown in Fig. S2 of the Supplementary Materials are similar to ones of KCC−4 and KCK−2.5.

Table 1 summarizes the textural parameters of the silica gel samples calculated from the isotherms. Here, V_s is the pore volume obtained from nitrogen adsorption at $p/p_0 = 0.99$ (relative uncertainty ±2%), S_{BET} is the surface area from the BET model (relative uncertainty ± 3%). $D_{BET} = 4\ V_s/S_{BET}$ is the average pore diameter according to the cylindrical pore model, while D_{ads} and D_{des} are the median pore diameters calculated from the adsorption and desorption branches of the isotherms and roughly representing the sizes of pore voids and pore necks, respectively. The micropore volume from the *t-plot* method does not exceed 0.01 $cm^3.g^{-1}$ for all studied samples. Thus, the micropores should not have significant influence on the bulk properties of silica gels.

Table 1
Textural parameters of silica gels.

Silica gel	S_{BET}, $m^2\cdot g^{-1}$	V_s, $cm^3\cdot g^{-1}$	D_{BET}, nm	D_{ads}, nm	D_{des}, nm
KCC−4	535	0.67	5.0	5.6	4.8
Sil−60	433	0.76	7.0	7.9	6.6
KCK−2.5	363	0.97	10.6	15.0	11.5
Sil−100	211	1.01	19.1	22.7	14.9
CX−120	134	0.69	20.6	41.2	26.1

To analyze the dependencies of dielectric permittivity on the silica pore size we used the parameter D_{BET}, which represents the ratio of pore volume to its surface area. Usually, the value of D_{BET} for silica gels with the mesopores of irregular pore shape is in the range given by D_{ads} and D_{des}. However, for KCK−2.5 and CX−120 with relatively large pores, D_{BET} is lower than D_{des}. The latter can probably be attributed to the presence of both the micropores and the nanoscale roughness of the mesopores' inner surface.

3.2. Thermal analysis

The PEG−400 content in the porous matrix was determined thermogravimetrically (Fig. S3). In Fig. S3, the relative mass loss vs temperature was plotted. This accounted for the following types of mass losses: 1) the adsorbed water m(H_2O) caught by samples during the manufacturing process and subsequent storage, 2) PEG−400, and 3) *-OH* surface groups on the silica gel surface. The mass content of the components is summarized in Table 2.

The uncertainties of the values in Table 2 are determined by the accuracy of the mass measurements and constitute ± 0.1% of the sample's mass.

The data in Table 2 indicate that the PEG−400 content in all samples is practically identical. The data also indicate the presence of a small amount of water in the samples. As even a low water content can significantly affect the properties of the composites, all samples were

Table 2
Mass fractions of samples' components calculated from mass loss dependencies.

Composite	m (H_2O), %	m (PEG−400), %	m (*-OH*), %
KCC−4/PEG−400	3.3	28.4	4
Sil−60/PEG−400	3.3	27.7	3.8
KCK−2.5/PEG−400	3.5	28.6	2.5
Sil−100/PEG−400	5.3	28.1	2.2
CX−120/PEG−400	5.5	28.1	1.1

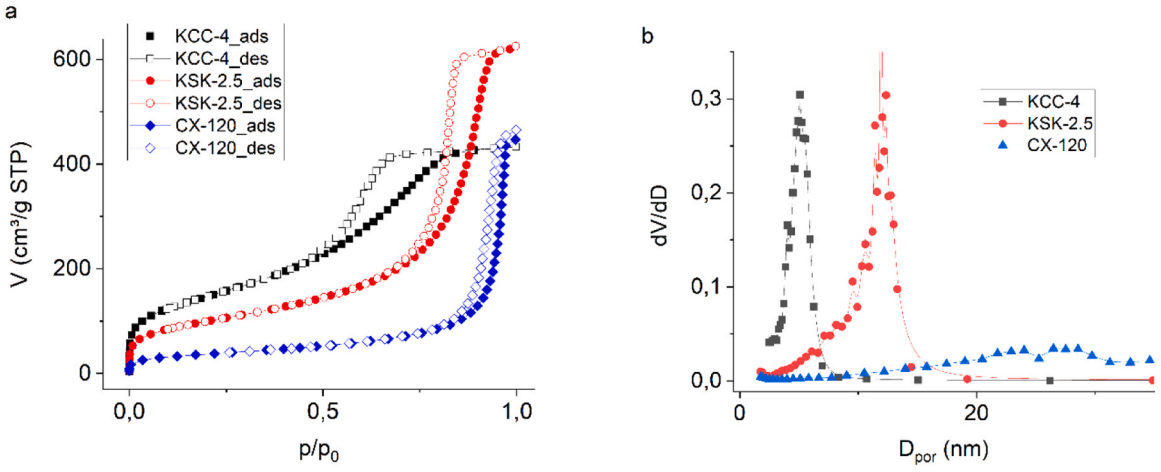

Fig. 2. Adsorption/desorption nitrogen isotherms (a) and pore size distributions via BJH, desorption (b) for KCC−4, KCK−2.5, CX−120 matrices.

dried prior to measurements. The A&D MX−50 moisture analyzer used for this task determines the amount of water eliminated from the sample.

3.3. Powder X-Ray diffraction

The structure of PEG−400 as a bulk solid and as confined within silica gel pores was elucidated by powder XRD. The X-ray diffraction patterns of PEG−400 at −50 °C were collected over the angular range of 10–40°. Fig. 3a shows that bulk PEG−400 exhibits two maxima at 19.5° and 23.2°, characteristic of a crystalline structure [28]. The pattern also contains a wide amorphous halo. Consequently, at −50 °C bulk-PEG−400 is in an amorphous-crystalline state with a degree of crystallinity equal to 9.5%.

The XRD patterns for both KCK−2.5/PEG−400 and Sil−100/PEG−400 samples reveal only wide halos with no sharp peaks (Fig. 3b), suggesting that PEG−400 in pores at −50 °C is amorphous.

3.4. Dielectric properties

The dielectric properties of the samples were measured by recording the temperature dependencies of the real and imaginary parts of the dielectric permittivity at 5, 10, 20, and 50 kHz frequencies of the external field oscillations.

The real part of the complex dielectric permittivity for bulk PEG−400 reveals an inflection in the −70 to −10 °C temperature region (Fig. 4a). This inflection point shifts towards higher temperatures at higher frequencies of the external field oscillation. The imaginary part of the complex dielectric permittivity exhibits a sharp peak in the same temperature range at 5 kHz frequency (Fig. 4b). This peak also shifts towards higher temperatures at higher frequencies. Such behavior is typical of samples undergoing dielectric relaxation in the aforementioned temperature range. This low-temperature relaxation in bulk PEG−400 can be attributed to the conformation motion of its *HO-CH_2-CH_2-* end groups [23].

A similar dielectric relaxation process is observed for PEG−400 confined in KCC−4 pores (Fig. 5). However, both its position and intensity are different compared to what is observed for bulk PEG−400. The temperature ranges, in which the relaxation process is observed, appear to be determined by pores' sizes in which the polymer is confined.

Overall, PEG−400 samples in pores exhibit a low-temperature dielectric relaxation, whose intensity and position appear to be determined by pore sizes. The data illustrating these trends are summarized in Figs. S 4–7 in the Supplementary Materials.

4. Discussion

To derive the relation between the pore size, the dielectric relaxation intensity and temperature for PEG−400, we can plot a temperature dependence of the real and imaginary parts of the complex dielectric permittivity for bulk PEG−400 and all PEG−400 in pores at 10 kHz external field oscillation frequency (Fig. 6). Based on these graphs, two qualitative trends emerge. First, the position of the dielectric relaxation region shifts towards higher temperatures with decreasing pore sizes. Second, the intensity of the dielectric relaxation decreases with decreasing pore sizes.

To analyze these trends quantitatively, we can plot the position of the dielectric relaxation as a function of the inverse pore size (Fig. 7). The position of the dielectric relaxation is deduced from the maxima positions on the imaginary part of the complex dielectric permittivity vs. temperature dependencies. The low-temperature dielectric relaxation in PEG−400 appears to shift towards higher temperatures with decreasing sizes of inclusions.

Further insights into the properties of the nano-structured PEG−400 in pores and the explanation of the phenomena described above can be drawn from the dielectric data obtained. As indicated earlier, the low-temperature relaxation in PEG−400 is due to thermal (relaxational) dipole polarization caused by conformational motion of the end groups, which 'unfreeze' when PEG−400 is heated. From here we can stipulate that such motion leads to the thermal dipole polarization and thus can be described using a two-level relaxator model.

In this model, each particle (e.g., a dipole in a polymer matrix) can occupy one of two energy states: a lower energy state and an excited state, whose energy is higher by V joules. The transition between these two states is driven by thermal fluctuations and involves overcoming an energy barrier of energy U. The Boltzmann distribution governs the populations of these levels, and thus this model allows for the description of the system's dielectric response via the statistics of transitions between these two states. The difference between the static (ε_s) and high-frequency (ε_∞) dielectric permittivities (the increment of the dielectric permittivity) can then, for the system with two energy levels, be written as [29]:

$$\Delta\varepsilon = \varepsilon_s - \varepsilon_\infty = \frac{N\mu^2}{3k\varepsilon_0 T} \bullet \frac{\exp\left(-\frac{V}{kT}\right)}{\left(1 + \exp\left(-\frac{V}{kT}\right)\right)^2} \quad (1)$$

where N is the number of dipoles in the system, μ is the difference in the relaxators dipole moments in position 1 and 2, k is the Boltzmann's constant, ε_0 is the permittivity of free space, and V is the difference in the energies of the ground and excited states.

Expression (1) has two interesting features: first, it directly relates

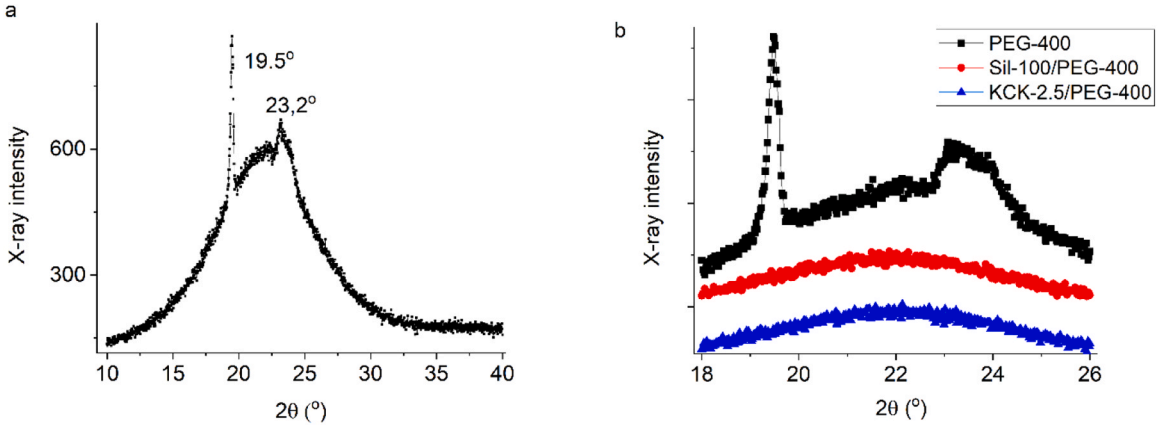

Fig. 3. Powder XRD patterns, recorded at −50 °C for: a. bulk-PEG−400, b. bulk- PEG−400, KCK−2.5/PEG−400, Sil−100/PEG−400.

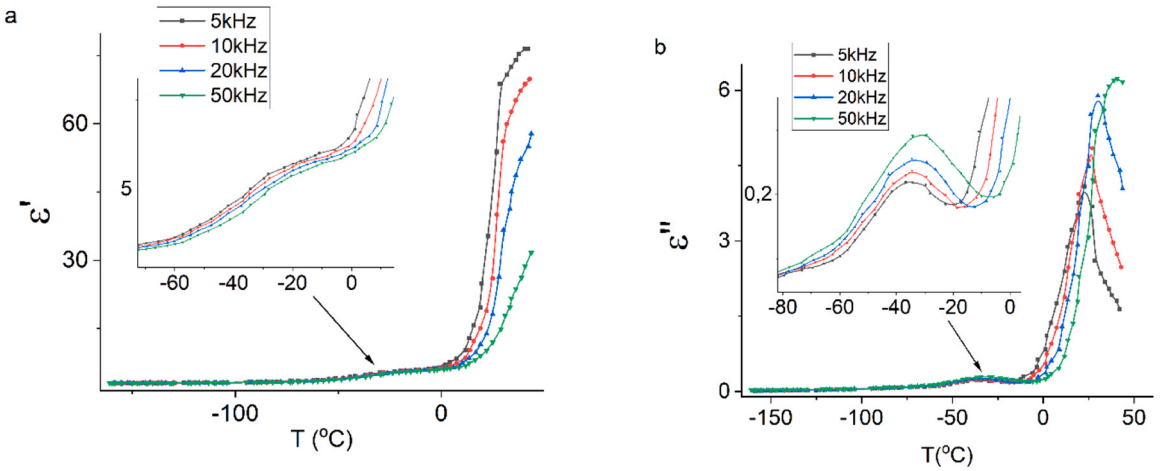

Fig. 4. Temperature dependences of the real (a) and imaginary (b) parts of the complex dielectric permittivity of PEG−400 at different frequencies.

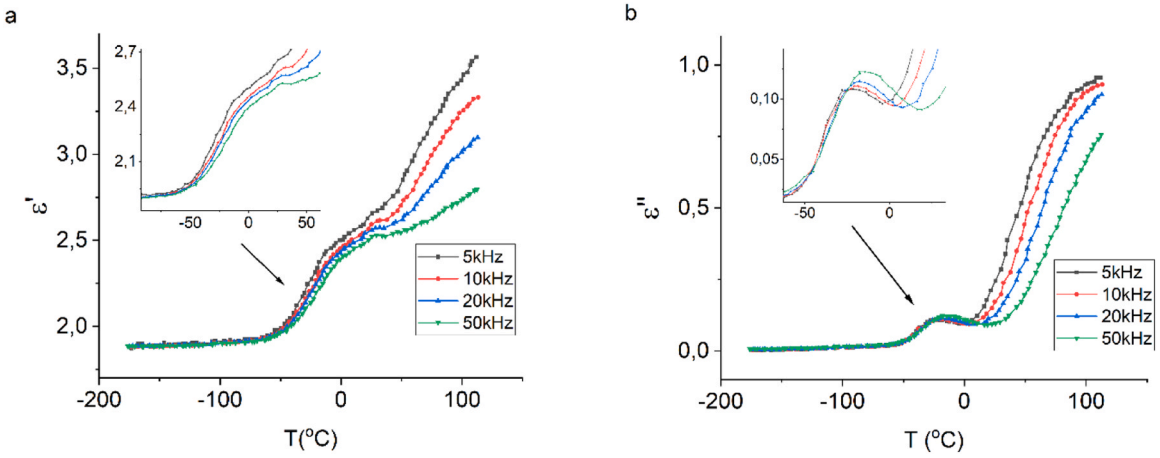

Fig. 5. Temperature dependences of the real (a) and imaginary (b) parts of the complex dielectric permittivity of PEG−400 in KCC−4 pores at different frequencies.

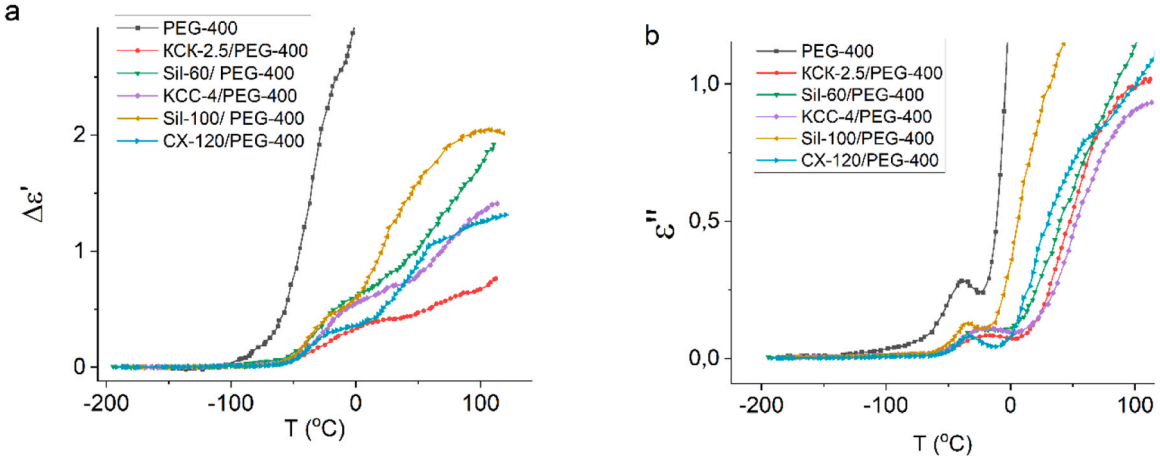

Fig. 6. Temperature dependences of the increments of the real (a) and imaginary parts (b) of the complex dielectric permittivity for all samples at 10 kHz frequencies.

the increase in the dielectric permittivity to the change in the dipole moment; second, it is a function of temperature (due to the populations of the two states).

The relaxation time necessary for the system to attain an equilibrium state is given by:

$$\tau = \tau_0 \bullet \exp\left(\frac{U - T\Delta S}{kT}\right), \quad (2)$$

where τ_0 is equal to 10^{-14} s (as estimated in [30]), U is the activation energy, and ΔS is the activation entropy.

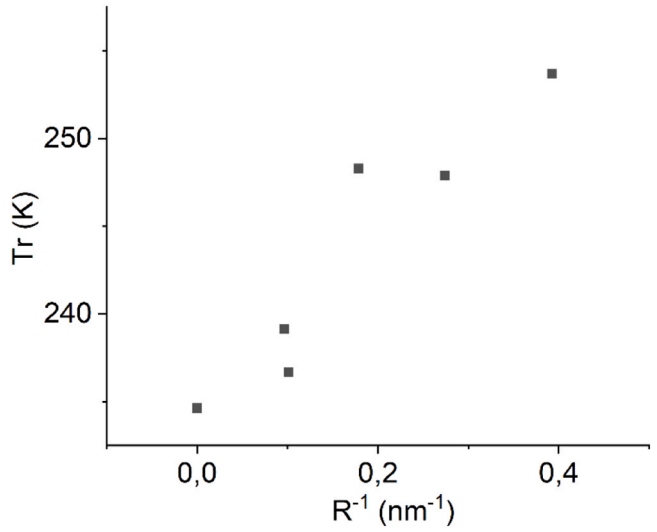

Fig. 7. Position of the maxima on the imaginary part of the complex dielectric permittivity vs. temperature dependencies for PEG−400 plotted for different values of the inverse pore radii.

The latter expression shows that the relaxation time depends on both the height of the energy barrier and the number of possible micro-configurations of the system (via the entropy term).

The maxima of the imaginary part of the complex dielectric permittivity $\varepsilon''(T, f)$ are attained for $\omega\tau = 1$. This leads to the Arrhenius equation:

$$lnf = \ln(2\pi\tau_0) + \frac{\Delta S}{k} - \frac{U}{kT}, \quad (3)$$

where f is the frequency of the external electric field oscillation.

The latter equation allows for the calculation of activation energy and activation entropy from the experimental data. To do so, the graphs of the ln *f* vs. inverse of the relaxation maximum temperature (1/Tr) were plotted for all samples (Fig. 8).

These experimental data were then fitted to Eq. (3), and the values of the activation energy U and the activation entropy ΔS/k are summarized in Table S1 (Supplementary Materials).

Both the activation energy (Fig. 9a) and the activation entropy (Fig. 9b) appear to vary inversely with pore size.

We attribute this behavior to the increasing influence of the pore walls on the polymer embedded within the pores. The smaller the pore is, the greater the percentage of the embedded molecules that interact with the walls of the pore.

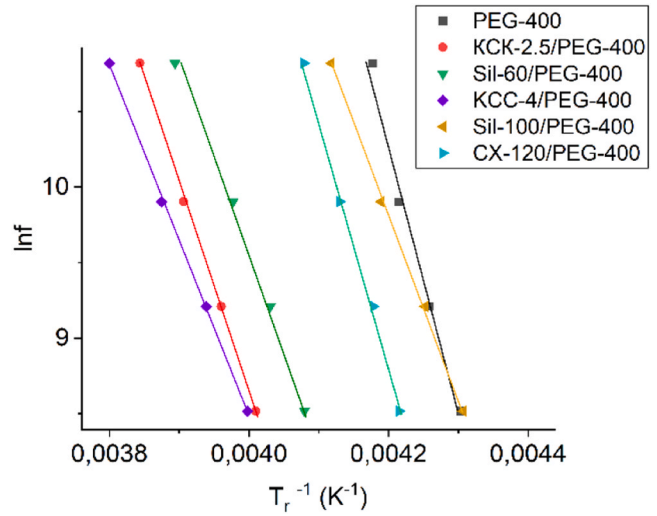

Fig. 8. The lnf(1/Tr) dependencies for the studied samples.

To gain further insight into the properties of PEG−400 in pores, we can observe the behavior of the dielectric permittivity increment in the temperature region where, according to (1), it plateaus. In order to determine the impact of the dielectric relaxation attributed specifically to PEG−400, we studied the thermal dependence of the complex dielectric permittivity for the KCK−2.5 matrix filled with octadecane (Fig.S8 in the supplementary). This allowed us to exclude the impact of the adsorbed water. Solid octadecane is known not to undergo dielectric relaxation in solid state. As the Fig S8 indicates, a dielectric relaxation is observed in the temperature range between −130 to −85 °C due to the silanol groups of silica gel. However, the temperature range of this relaxation does not overlap with the dielectric relaxation region for PEG, and thus does not affect the increment of the dielectric relaxation in PEG.

To describe the behavior of the increment of the dielectric permittivity using expression (1), we identified the increment of the dielectric permittivity due to dielectric relaxation in PEG in silica gel matrix (Fig. S9). We then identified the plateau region, as shown in Fig S9 and described it using (1).

The numeric values of these quantities are summarized for all samples in Table S1. As both quantities appear to vary with decreasing pore sizes, we can plot $N\mu^2$ (Fig. 10a) and V (Fig. 10 b) vs. inverse pore size.

Assuming the number of dipoles of the PEG−400 per unit volume is constant across samples with different pore sizes, the constant values of $N\mu^2$ independent of the inverse pore size indicate that the dipole moment of the PEG−400 remains unchanged as the relaxator transitions from equilibrium state 1 to equilibrium state 2. It is, however, also possible, that as the size of the inclusion changes, the number of dipoles changes as well. This implies that the change in the dipole moment for different samples will be different. The question of how to determine the concentration of dipoles in the inclusion remains, to our best knowledge, unanswered. We hope to address it in our future work.

Fig. 10b suggests that as the size of the inclusion decreases, the difference V increases as well. The numerical values of *V* can serve as indicators of the intensity of thermally activated motion. The relationship between V and the pore size was derived in [31]:

$$V = V_0\left[1 - \frac{13}{18}\left(\frac{a}{R}\right)^3\right] \quad (4)$$

where V_0 is the value of V in the limiting case of the size of nanoinclusion approaching infinity, R is the radius of the nanoinclusion, and *a* is the radius of the activation zone inside the nanoinclusion. The activation zone is the region within the nanoinclusion affected by the reorientation of dipoles during their transition between equilibrium positions.

If we now fit the V(1/R) data in Fig. 10b with Eq. (4), we can obtain the numerical values of $a = 3.13$ nm and $V_0 = 7.6$ kJ.mol^{-1}.

The size of the activation zone *a* appears to be comparable with the pore sizes, so we can assume that any pore contains a single activation zone and these activation zones are physically isolated from one another.

The activation entropy values can be further used to determine the number of excited relaxators in an activation zone [30]

$$\Delta S = k_B \ln \frac{Q!}{n!(Q-n)!} \quad (5)$$

where *Q* is the number of dipoles in the activation zone, *n* is the number of dipoles in the excited state, and Q−n is the number of dipoles in the ground state within the activation zone. We then calculated the number of dipoles in the activation zone. To do so we assumed the activation zone to be cubic with side $2a = 6.26$ nm and volume $V_a = 245.31$ nm^3. The volume of PEG−400 molecule was assumed to be a right prism of square base with side 0.443 nm and height 2.5 nm. This volume is V_m

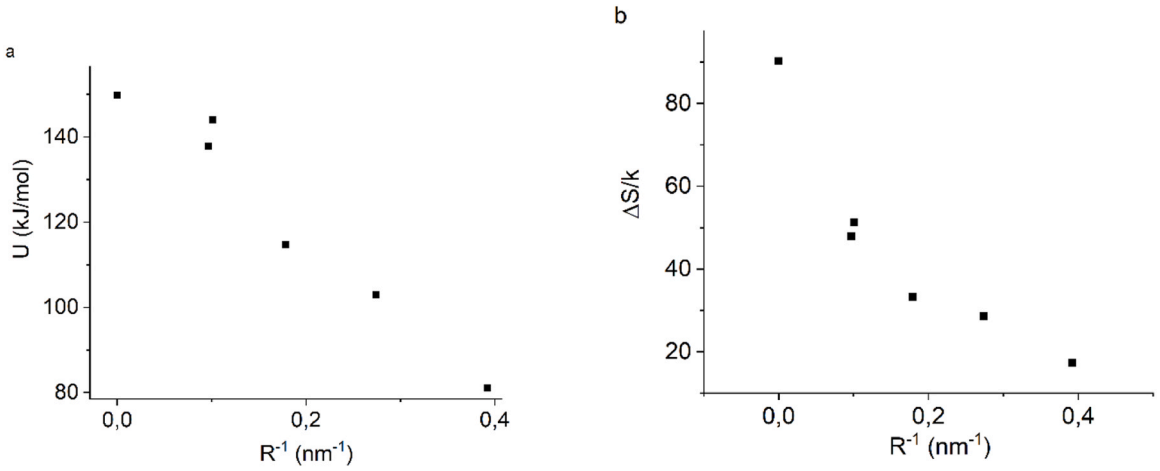

Fig. 9. Activation energy (a) and activation entropy (b) vs. inverse pore size.

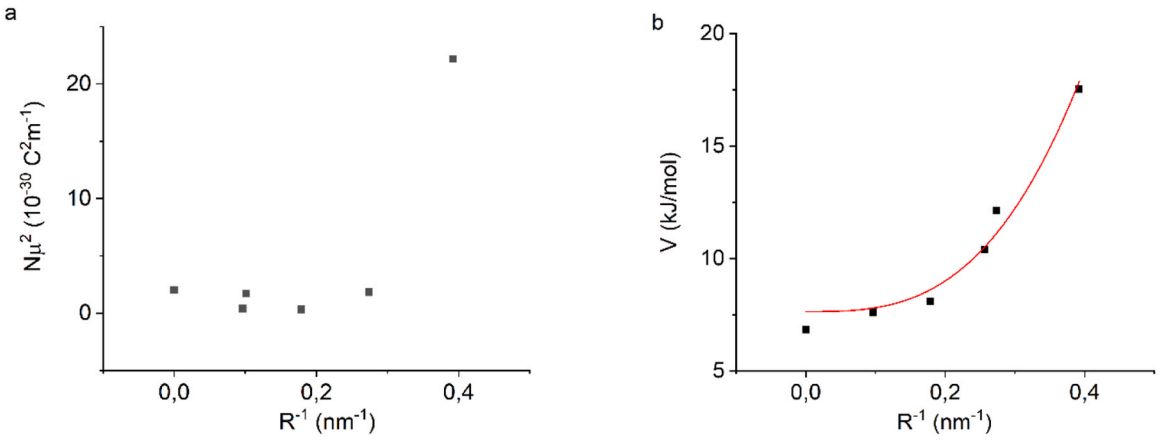

Fig. 10. The values of parameters $N\mu^2$ (a) and V (b) vs. inverse pore size.

$= 0.49\ nm^3$. Assuming that a reorienting dipole is associated with an end group, and that a molecule has two end groups, the number of dipoles can be deduced using the following formula:

$$Q = 2\ V_a / V_m = 1002$$

The number of dipoles can be calculated as the ratio of the volume of the activation zone and the volume of a single dipole. The experimental values of ΔS can then be used to determine the number of simultaneously activated relaxators in an activation zone and plotted against the inverse pore size (Fig. 11a). This number appears to decrease with decreasing pore size.

We can finally estimate the energy gained by a relaxator in an activated state. If n relaxators are activated simultaneously and the activation energy is U, then the energy gained by a single relaxator in an excited state is

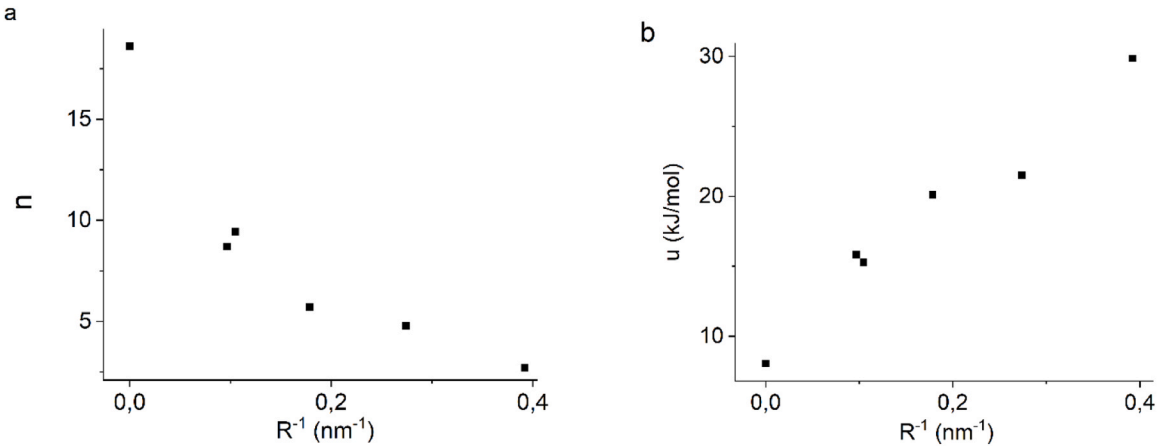

Fig. 11. The number of simultaneously activated relaxators n (a) and the energy of the excited relaxator u (b) vs. inverse pore size.

$$u = U/n \quad (6)$$

The value of u is plotted for different inverse pore sizes in Fig. 11b. The energy of the excited relaxators appears to increase with decreasing pore sizes. In other words, the wall's impact on the relaxator increases with decreasing pore size, driving the energy of the relaxator necessary to transition into the excited state higher. This, in turn, shifts the dielectric relaxation of the PEG−400 confined in smaller pores towards higher temperatures.

5. Conclusions

So, what is the impact of the porous matrix on the low-temperature dielectric relaxation of the PEG−400 inclusions? When nano-inclusions of PEG−400 are cooled in the silica gel pores, they form an amorphous phase (in sharp contrast with the bulk PEG−400, which forms an amorphous-crystalline phase at low temperatures). As the nano-inclusions are heated, they undergo a low-temperature dielectric relaxation which shifts towards higher temperatures at smaller inclusion sizes. At the same time, the activation energy and the activation entropy appear to decrease for smaller inclusions. The latter can be explained by the role the pore walls play in determining the structure of the nano-inclusions. The interaction with pore walls also increases the difference between the energies in the relaxator's equilibrium states. The interaction with the wall in smaller pores also decreases the number of simultaneously activated relaxators, as the energy required for a relaxator to transition into the excited state increases.

The obtained results may be relevant in the context of emerging Industry 6.0 concepts, where intelligent manufacturing, artificial intelligence, and machine learning are increasingly applied for the design and optimization of advanced functional materials [32]. In particular, the established relationship between pore size, interfacial interactions, and dielectric relaxation parameters in silica gel–PEG systems provides a physically grounded dataset that could be further utilized for AI-assisted prediction and digital optimization of nanostructured materials with programmable dielectric behavior. Such approaches are considered important elements of next-generation intelligent and sustainable manufacturing frameworks associated with Industry 6.0, where data-driven materials engineering and adaptive multifunctional systems play a key role [32].

The present study may also be viewed in the broader context of sustainable development and climate-oriented materials science associated with the United Nations Sustainable Development Goals (SDGs) [33]. Understanding the relationship between nanoscale confinement, interfacial interactions, and dielectric behavior in silica gel–PEG systems contribute to the development of advanced functional nanomaterials with controllable thermal and dielectric responses, which are important for energy-efficient electronic, sensing, and smart material applications. Such materials engineering approaches are increasingly recognized as crucial for sustainable technological development and climate resilience, especially in the field of nanotechnology and environmentally adaptive materials systems [34].

CRediT authorship contribution statement

Filip Ublekov: Investigation, Data curation. **Neli Koseva:** Investigation, Data curation. **Yaremov P. S.:** Investigation, Data curation. **Shvets O. V.:** Investigation, Data curation. **Alekseev O. M.:** Conceptualization. **Lazarenko Maksym:** Writing – review & editing, Supervision, Project administration, Data curation. **Sobchuk A. O.:** Writing – original draft, Investigation, Data curation. **Shevchenko V. B.:** Investigation, Data curation. **Alekseev S. A.:** Investigation, Data curation. **Yablochkova K .S.:** Writing – review & editing, Investigation. **Lysenkov E. A.:** Writing – original draft, Investigation. **Dinzhos R. V.:** Investigation, Data curation.

Declaration of Competing Interest

The authors declare that they have no known competing financial interests or personal relationships that could have appeared to influence the work reported in this paper.

Acknowledgements

This work has been supported by Ministry of Education and Science of Ukraine, Grant № 0125U002258.

Appendix A. Supporting information

Supplementary data associated with this article can be found in the online version at doi:10.1016/j.nxmate.2026.102511.

References

[1] P. Huber, Soft matter in hard confinement: phase transition thermodynamics, structure, texture, diffusion and flow in nanoporous media, J. Phys. Condens. Matter 27 (2015) 103102, https://doi.org/10.1088/0953-8984/27/10/103102.
[2] Q. Jiang, M.D. Ward, Crystallization under nanoscale confinement, Chem. Soc. Rev. 43 (2014) 2066–2079, https://doi.org/10.1039/C3CS60234F.
[3] A. Schönhals, H. Goering, C. Schick, B. Frick, R. Zorn, Glass transition of polymers confined to nanoporous glasses, Colloid Polym. Sci. 282 (2004) 882–891, https://doi.org/10.1007/s00396-003-1035-2.
[4] M.M. Lazarenko, A.N. Alekseev, S.A. Alekseev, Y.E. Grabovsky, M.V. Lazarenko, K. I. Hnatiuk, Structure and thermal motion of 1-octadecene confined in the pores of porous silicon, Mol. Cryst. Liq. Cryst. 660 (2018) 123–130, https://doi.org/10.1080/15421406.2017.1362250.
[5] K.I. Hnatiuk, R.V. Dinzhos, M.S. Simeonov, A.N. Alekseev, S.A. Alekseev, V. V. Sirko, Yu.F. Zabashta, N.S. Koseva, M.M. Lazarenko, Melting of 1-octadecene inside the pores of open-morphology silica gel: thermodynamic model and experimental studies, J. Therm. Anal. Calorim. 141 (2020) 1243–1250, https://doi.org/10.1007/s10973-019-08933-5.
[6] L.A. Bulavin, O.M. Alekseev, Y.F. Zabashta, M.M. Lazarenko, Phase equilibrium, thermodynamic limit, and melting temperature in nanocrystals, Ukr. J. Phys. 63 (2018) 1036–1040.
[7] C.M. Costa, R. Sabater i Serra, A. Andrio Balado, J.L. Gómez Ribelles, S. Lanceros-Méndez, Dielectric relaxation dynamics in poly(vinylidene fluoride)/Pb($Zr_{0.53}Ti_{0.47}$)O_3 composites, Polymer 204 (2020) 122811, https://doi.org/10.1016/j.polymer.2020.122811.
[8] J. Gao, W. Tao, D. Chen, X. Guo, Y. Chen, Y. Jiang, High performance shape-stabilized phase change material with nanoflower-like wrinkled mesoporous silica encapsulating polyethylene glycol: preparation and thermal properties, Nanomaterials 8 (2018) 385, https://doi.org/10.3390/nano8060385.
[9] K. Kumbhakar, T.D. Pham, K.-K. Lee, K. Kwak, M. Cho, Dielectric relaxation spectroscopy for the characterization of ion transport in solid polymer electrolytes in Li-ion cells, Electrochim. Acta 462 (2023) 142759, https://doi.org/10.1016/j.electacta.2023.142759.
[10] J. Schüller, R. Richert, E.W. Fischer, Dielectric relaxation of liquids at the surface of a porous glass, Phys. Rev. B 52 (1995) 15232–15240, https://doi.org/10.1103/PhysRevB.52.15232.
[11] J. Son, H. Park, M. Kim, J.H. Park, K.-H. Nam, J.-S. Bae, Frequency-Dependent Dielectric Permittivity and Water Permeability in Ordered Mesoporous Silica-Grafted Fluorinated Polyimides, Polymers 16 (2024) 1716, https://doi.org/10.3390/polym16121716.
[12] V. Shevchenko, A. Sobchuk, O.M. Alekseev, S.A. Alekseev, E. Lysenkov, R.V. Dinzhos, T. Budnyak, O. Tkachenko, M.M. Lazarenko, Effect of PEG 400 nanocrystal sizes on thermal and spectral properties, in: Proc. IEEE 14th Int. Conf. Nanomaterials: Applications and Properties (NAP), 2024, 10739716. https://doi.org/10.1109/NAP62956.2024.10739716.
[13] F.M. Coelho, L.F. Mercier Franco, The Interplay between Dynamics and Structure on the Dielectric Tensor of Nanoconfined Water: Surface Charge and Salinity Effect, J. Phys. Chem. B 128 (2024) 11759–11767, https://doi.org/10.1021/acs.jpcb.4c05803.
[14] S. Napolitano, M. Wübbenhorst, The lifetime of the deviations from bulk behaviour in polymers confined at the nanoscale, Nat. Commun. 2 (2011) 260, https://doi.org/10.1038/ncomms1259.
[15] M. Solar, K. Binder, W. Paul, Relaxation processes and glass transition of confined polymer melts: A molecular dynamics simulation of 1,4-polybutadiene between graphite walls, J. Chem. Phys. 146 (2017) 203308, https://doi.org/10.1063/1.4975390.
[16] S. Cheng, S. Mirigian, J.M.Y. Carrillo, V. Bocharova, B.G. Sumpter, K.S. Schweizer, A.P. Sokolov, Revealing spatially heterogeneous relaxation in a model nanocomposite, J. Chem. Phys. 143 (2015) 194704, https://doi.org/10.1063/1.4935171.
[17] C. Gainaru, S. Schildmann, R. Böhmer, Surface and confinement effects on the dielectric relaxation of a monohydroxy alcohol, J. Chem. Phys. 135 (2011) 174510, https://doi.org/10.1063/1.3655356.

[18] N.R. Aluru, et al., Fluids and electrolytes under confinement in single-digit nanopores, Chem. Rev. 123 (2023) 2737–2831, https://doi.org/10.1021/acs.chemrev.2c00155.
[19] E.A. Lysenkov, I.P. Lysenkova, V.V. Klepko, Relaxation processes in nanocomposite polymer electrolytes based on polyethylene glycol and hybrid nanofiller. Proceedings of the IEEE International Conference on Electronics and Nanotechnology (ELNANO), 2020, pp. 134–137, 10.1109/ELNANO50318.2020.9088895.
[20] G.T. Nguyen, Polyethylene glycol/fumed silica composites as shape-stabilized phase change materials with effective thermal energy storage, RSC Adv. 13 (2023) 7621–7631, https://doi.org/10.1039/D2RA08134B.
[21] S. Wang, C. Wang, P. Takyi-Aninakwa, S. Jin, C. Fernandez, Q. Huang, An improved parameter identification and radial basis correction-differential support vector machine strategies for state-of-charge estimation of urban-transportation-electric-vehicle lithium-ion batteries, J. Energy Storage 80 (2024) 110222.
[22] A. Schönhals, R. Stauga, Broadband dielectric study of anomalous diffusion in a poly(propylene glycol) melt confined to nanopores, J. Chem. Phys. 108 (1998) 5130–5136, https://doi.org/10.1063/1.475918.
[23] M.M. Lazarenko, O. Sobchuk, D.A. Andrusenko, V.B. Shevchenko, S.A. Alekseev, K. S. Yablochkova, E.A. Lysenkov, R.V. Dinzhos, F. Ublekov, P. Tuleshkov, N. Koseva, N.M. Gregirchak, M.V. Lazarenko, O.M. Alekseev, M.M. Lazarenko, Investigation of relaxation processes and phase transition in the polyethylene glycol 400 using IR spectra in a wide temperature range, Low. Temp. Phys. 51 (2025) 231–238, https://doi.org/10.1063/10.0035407.
[24] A.N. Alekseev, M.M. Lazarenko, M.V. Lazarenko, K.N. Kovalev, S.Y. Tkachev, Characterization of dielectric properties in liquid–solid phase transition, Inorg. Mater. 53 (2017) 1473–1477, https://doi.org/10.1134/S002016851715002X.
[25] O.M. Alekseev, M.M. Lazarenko, G.O. Puchkovs'ka, T.V. Bezrodnaya, A. A. Sendzyuk, Peculiarities of the thermal motion in crystals formed by cetyltrimethylammonium bromide molecules, Ukr. J. Phys. 55 (2010) 973–978.
[26] K.S.W. Sing, D.H. Everett, R.A.W. Haul, L. Moscou, R.A. Pierotti, J. Rouquerol, T. Siemieniewska, Reporting physisorption data for gas/solid systems, Pure Appl. Chem. 57 (1985) 603–619.
[27] M. Thommes, K. Kaneko, A.V. Neimark, J.P. Olivier, F. Rodriguez-Reinoso, J. Rouquerol, K.S.W. Sing, Physisorption of gases, with special reference to the evaluation of surface area and pore size distribution (IUPAC Technical Report), Pure Appl. Chem. 87 (2015) 1051–1069, https://doi.org/10.1515/pac-2014-1117.
[28] B.S. Bhatnagar, S.M. Martin, D.L. Teagarden, E.Y. Shalaev, R. Suryanarayanan, Investigation of PEG crystallization in frozen PEG–sucrose–water solutions: II. Characterization of the equilibrium behavior during freeze–thawing, J. Pharm. Sci. 99 (2010) 4510–4524, https://doi.org/10.1002/jps.22186.
[29] M.M. Lazarenko, A.N. Alekseev, S.A. Alekseev, K.I. Hnatiuk, O.F. Demidiuk, K. S. Yablochkova, N.O. Atamas, M.V. Lazarenko, Topological solitons in chain molecular crystals with stoichiometric obstacles and hydrogen bonds, J. Phys. Chem. Solids 144 (2020) 109514, https://doi.org/10.1016/j.jpcs.2020.109514.
[30] M.M. Lazarenko, Y.F. Zabashta, O.M. Alekseev, S.A. Alekseev, K.S. Yablochkova, L. Y. Vergun, D.A. Andrusenko, K.V. Cherevko, V.B. Shevchenko, R.V. Dinzhos, L.A. Bulavin, Thermally activated processes: the underlying mechanism of activated state formation, RSC Adv. 14 (2024) 39242–39252, https://doi.org/10.1039/D4RA05863A.
[31] K.I. Hnatiuk, Y.F. Zabashta, M.M. Lazarenko, S.A. Alekseev, K.S. Yablochkova, M. V. Ushcats, R.V. Dinzhos, L.Y. Vergun, D.A. Andrusenko, A.N. Alekseev, L.A. Bulavin, Dielectric relaxation in nanocrystals: a scale effect, J. Phys. Chem. C. 127 (2023) 12107–12117, https://doi.org/10.1021/acs.jpcc.3c02045.
[32] H. Majeed, T. Iftikhar, Intelligent Manufacturing in Industry 6.0: A Climate Resilience Approach, Springer Nature, 2026, https://doi.org/10.1007/978-3-032-07278-8.
[33] B. Elzein, Nano Revolution:"Tiny tech, big impact: How nanotechnology is driving SDGs progress, Heliyon 10 (2024) e31393, https://doi.org/10.1016/j.heliyon.2024.e31393.
[34] H. Majeed, T. Iftikhar, K. Maqsood, Synthesis of protein-based catalyst for multi-industrial applications by using agriculture and industrial waste, Polym. Bull. 81 (2024) 12633–12653, https://doi.org/10.1007/s00289-024-05302-0.